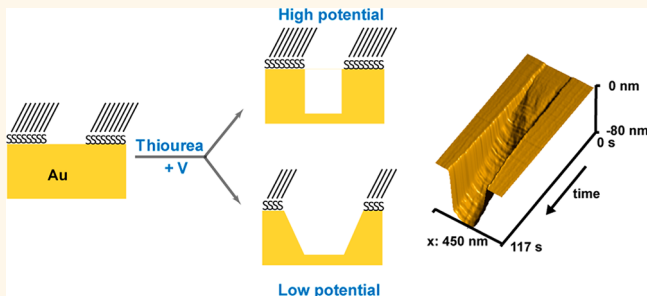


Electrochemical Etching of Gold within Nanoshaved Self-Assembled Monolayers

Jingru Shao,^{†,§} Eric A. Josephs,^{‡,§} Cheetar Lee,[†] Adriana Lopez,[†] and Tao Ye^{†,*}

[†]School of Natural Sciences and [‡]School of Engineering, University of California, Merced, California 95343, United States. [§]These authors contributed equally.

ABSTRACT Wet etching of metal substrates with patterned self-assembled monolayers (SAMs) is an inexpensive and convenient method to produce metal nanostructures. For this method to be relevant to the fabrication of high precision plasmonic structures, the kinetics of nanoscale etching process, particularly in the lateral direction, must be elucidated and controlled. We herein describe an *in situ* atomic force microscopy (AFM) study to characterize the etching process within patterned SAMs with nanometer resolution and in real time. The *in situ* study was enabled by several unique elements, including single crystalline substrates to minimize the variability of facet-dependent etch rate, high-resolution nanoshaved SAM patterns, electrochemical-potential-controlled etching, and AFM kymographs to improve temporal resolution. Our approach has successfully quantified the extent of both lateral etching and vertical etching at different potentials. Our study reveals the presence of an induction period prior to the onset of significant lateral etching, which would be difficult to observe with the limited time resolution and sample-to-sample variation of *ex situ* studies. By increasing the vertical etch rate during this induction period with higher potentials, gold was etched up to 40 nm in the vertical direction with minimal lateral etching. High-resolution etching was also demonstrated on single crystal gold microplates, which are high quality gold thin films suitable for plasmonics studies.



KEYWORDS: metal nanostructures · electrochemical etching · atomic force microscopy · alkanethiol self-assembled monolayers · thiourea · scanning probe lithography

The ability to concentrate, guide and modulate electromagnetic energy at the nanoscale with surface plasmons crucially depends on the shapes and sizes of noble metal nanostructures.¹ While relatively simple metallic structures are produced with chemical synthesis^{2,3} or template stripping,^{4,5} more complex structures, particularly those useful for plasmonic circuits, are commonly fabricated with focused-ion beam (FIB)^{6,7} and electron beam lithography (EBL).⁸ A potential alternative that is inexpensive, convenient, and less damaging to immobilized biomolecules in plasmonics-based biosensors^{4,9} is wet etching with patterned self-assembled monolayers (SAMs).^{10–13} Alkanethiol SAMs, which can be patterned using soft-lithography^{14,15} or scanning probe lithography,^{16–18} can protect the underlying noble metal while the metal in exposed areas is etched away by a chemical etchant. A major barrier to the fabrication of high-resolution metallic

nanostructures with wet etching is lateral etching that occurs at the boundaries of the exposed areas.^{10–13} To produce high-aspect ratio, nanometer-precision structures that are routinely required in plasmonics,^{19,20} the vertical etch rate, R_V , must be significantly larger than the lateral etch rate, R_L . Such high etching anisotropy is difficult to achieve with the polycrystalline gold thin films that are commonly used in wet etching studies.^{10–12} Moreover, our ability to improve pattern transfer fidelity is hampered by the limited knowledge of the wet etching process, as the elucidation of etching kinetics is hindered by the low time resolution in existing *ex situ* studies.^{10,12,13} In addition, due to the damage of the SAM resist by electron beams¹⁰ and contamination of gold by exposure in air,^{10,12,13} a fresh sample must be used for each time point in *ex situ* studies. Therefore, it is challenging to measure the extent of lateral etching with sub 10-nm precision due to the expected

* Address correspondence to tao.ye@ucmerced.edu.

Received for review March 20, 2013 and accepted May 28, 2013.

Published online May 28, 2013
10.1021/nn4014005

© 2013 American Chemical Society

sample-to-sample variability in the sizes of the SAM patterns and irregular etching of the polycrystalline substrate.

To understand and control the etching process for faithful pattern transfer on gold, we herein report the first *in situ* AFM study of electrochemical etching within a patterned SAM resist. This *in situ* study was made possible by addressing numerous technical barriers, including the variability of etch rates on different crystalline facets of polycrystalline gold films,^{10–12} lack of control over etching kinetics, and insufficient temporal resolution of AFM imaging. Our study successfully quantified both lateral and vertical etching with subsecond time resolution under potential control. Our results have indicated that the etching process is surface reaction limited and is affected by surface adsorbates. The etch rate is not constant even at a fixed electrode potential. Lateral etching has a pronounced induction period, which is attributed to the selective passivation of the sidewall. By controlling etching kinetics on different crystalline facets, we have identified the conditions needed to achieve high etching anisotropy—lateral etching is within the measurement error (4 nm) when gold is vertically etched below 40 nm. Our *in situ* approach may be readily used to study and control nanoscale etching kinetics with alkanethiol SAM resists produced by other patterning methods.^{12,15,21} In addition, our method may be used to produce complex, high-resolution plasmonic nanostructures that allow selective immobilization of biochemical ligands in “hot spots”.⁹

RESULTS AND DISCUSSION

Thus far, *in situ* scanning probe microscopy studies of etching of passivated gold surfaces are mostly limited to those with unpatterned SAMs.^{22,23} It has been found that the corrosion of gold preferentially initiates in SAM defects. Due to the low time resolution of imaging and limited control over the defects, these studies have largely focused on qualitative aspects of corrosion.^{22,23} For *in situ* microscopy to be relevant to pattern transfer with SAM resists, it is imperative to produce open gold areas in the SAM with high resolution and obtain quantitative information of lateral and vertical etching. Our approach integrated the following unique elements to overcome technical barriers to *in situ* imaging: (1) we used Au(111) substrates (a bulk single crystal²⁴ or gold microplates)²⁵ to avoid the variability of etch rates of polycrystalline gold films; (2) we patterned an alkanethiol SAM on gold by nanoshaving, which offers a resolution as high as 10 nm (Figure 1). During nanoshaving, the alkanethiol molecules are mechanically desorbed by a large local pressure applied by the AFM tip to expose the underlying gold surface (Figure 1a, left and middle);¹⁸ (3) while the introduction of a chemical oxidant into the liquid cell may perturb *in situ* imaging and allow for

limited control over the etching process, we applied an electrochemical potential to initiate the etching so that AFM could track the evolution of the nanoshaved area; (4) while traditional frame-by-frame imaging is too slow, we instead configured the AFM to scan the same line across the nanoshaved shapes repeatedly (Figure 1a, right). The topography profiles of the scanned line at different time points were stacked to form what we called AFM kymographs (as shown in Figure 1b and later), with the topography profile of the scanned line shown along x axis and the y axis representing time. The kymographs provided a convenient and intuitive method to quantify vertical and lateral etching with subsecond time resolution.

In Situ Measurement of Electrochemical Etching. We used octadecanethiol (C18) as the etch resist, as C18 SAMs have been previously shown to serve as a robust and high-quality wet etch resist.^{25,26} Then, using nanoshaving, we exposed nanoscale regions in the C18 SAM formed on the Au(111) substrate.²⁴ The sample was then exposed to the etchant: 40 mM thiourea in 10 mM sulfuric acid solution.²⁷ The reaction describing the etching of gold by thiourea in acidic solutions is as follows:²⁸



where TU represents the thiourea $\text{SC}(\text{NH}_2)_2$ and AuTU_2^+ represents the gold–thiourea complex. Thiourea must diffuse and adsorb onto the gold surface to form the aqueous species AuTU_2^+ with the aid of oxidant, which leads to etching of gold. While Fe^{3+} is often used as the oxidant for thiourea-mediated etching of gold,^{12,15,21} the introduction of a new oxidant into the liquid cell may perturb *in situ* imaging and require some stabilization time before images can be acquired reliably and a stable local concentration is established. Therefore, we used the electrochemical potential to initiate the oxidation/etching on demand so that the progression of etching at the bare gold region could be tracked *in situ* by AFM (Figure 1a, right, and 1b). As will be shown later, potential control also offers a unique opportunity to facilitate anisotropic etching.

Although we did not intentionally add an oxidant such as Fe^{3+} to the thiourea solution, we found that the nanoshaved areas were rapidly etched even without any applied potential (Figure 2a–c) or at -300 mV (data not shown). We suspected that the dissolved dioxygen may serve as the oxidant in the presence of thiourea.^{27,29} To test the hypothesis, a nanoshaved SAM surface was exposed to the thiourea solution that had been purged with nitrogen. Indeed, no etching was observed this time (Figure 2d–f). Therefore, by removing oxygen from the thiourea etchant, we can trigger the etching process with potential control.

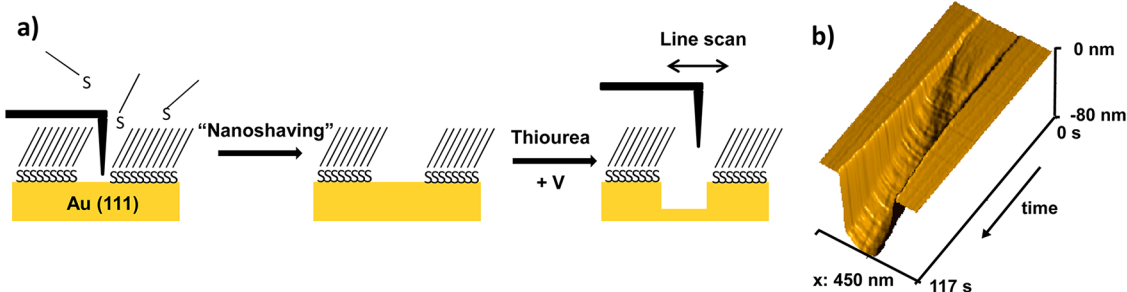


Figure 1. Schematic of *in situ* characterization of gold etching in nanopatterned SAM resist. (a) Octadecanethiol (C18) SAM on Au(111) is patterned by nanoshaving, which uses the pressure exerted by an AFM tip to selectively desorb thiol molecules in specific areas. The sample is then subjected to an acidic thiourea solution under electrochemical control. Etching at the nanoshaved area is triggered by applying a positive potential to the gold substrate, and AFM is used to image the nanoshaved area during etching. (b) 3D view of an AFM kymograph, which shows a nanoshaved region being gradually etched in both vertical and lateral directions. AFM repeatedly images the same line as etching proceeds and the topographical profiles are stacked together to form the AFM kymograph, with the Y axis representing the time axis.

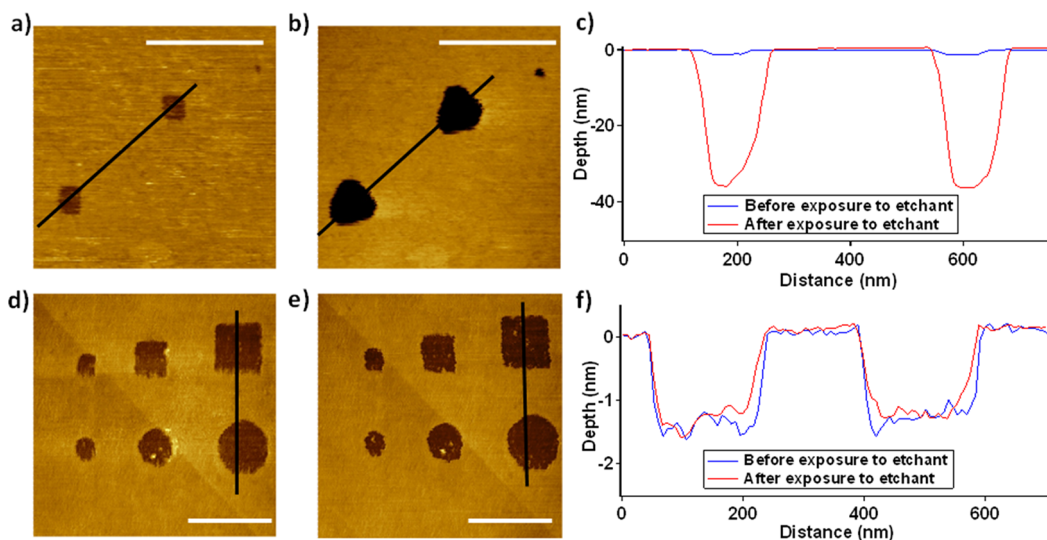


Figure 2. Role of air in the gold etching reaction. (a) AFM image of the nanoshaved patterns in butanol. The depth was about 1.5 nm. (b) After exposing the surface to aerated thiourea solution for a minute, the nanoshaved areas were etched to 35 nm deep and turned into triangular/hexagonal shapes at open circuit potential. The edges of the deeply etched holes are along the nearest neighbor directions of Au(111). (c) Cross-sectional profiles of the pattern in panel a (blue) and panel b (red). (d) AFM image of the shaved patterns before and (e) after exposure to deaerated thiourea solution. (f) Cross-sectional profiles of nanoshaved holes in panel d (blue) and panel e (red) show identical depths, suggesting that etching is minimal under this condition. Scale bars are 300 nm.

To study the etching kinetics with kymograph, we configured the AFM to scan the same line across the nanoshaved region repeatedly. As there was no lateral etching in the overall shape if lateral etching was not observed in the kymograph (Figure S1), the measured depths and widths in the kymograph could therefore be used to monitor the etching kinetics of the shape of interest with a lateral precision of ~ 4 nm (AFM measurement error, see Materials and Methods section for discussion) and a vertical precision of 0.27 nm. This approach, which allows us to determine etching anisotropy with subsecond time resolution, represents an optimum balance between temporal resolution and topographical information needed to understand the nanoscale etching process. To address the potential concern that tapping mode imaging by the AFM tip

may perturb the etching process, we imaged the nanoshaved shapes after etching (Figure S2). There was no observed depth difference between the AFM scanned line and the rest of the shaved area. In addition, the shapes that were imaged by the tip and those that were not imaged were etched to the same depth. These observations suggest that the tapping mode imaging used to characterize the etching minimally perturbs the electrode reactions. The lack of tip perturbation is also an indication that the etching process is limited by surface reaction, not mass transport of reactants, which is impeded by the presence of the AFM tip. Indeed, our estimated etch rates under a mass transport limited scenario (modeled as a recessed micro-disk electrode) are at least 3 orders of magnitude higher than our measured etch rates (Supporting Information).

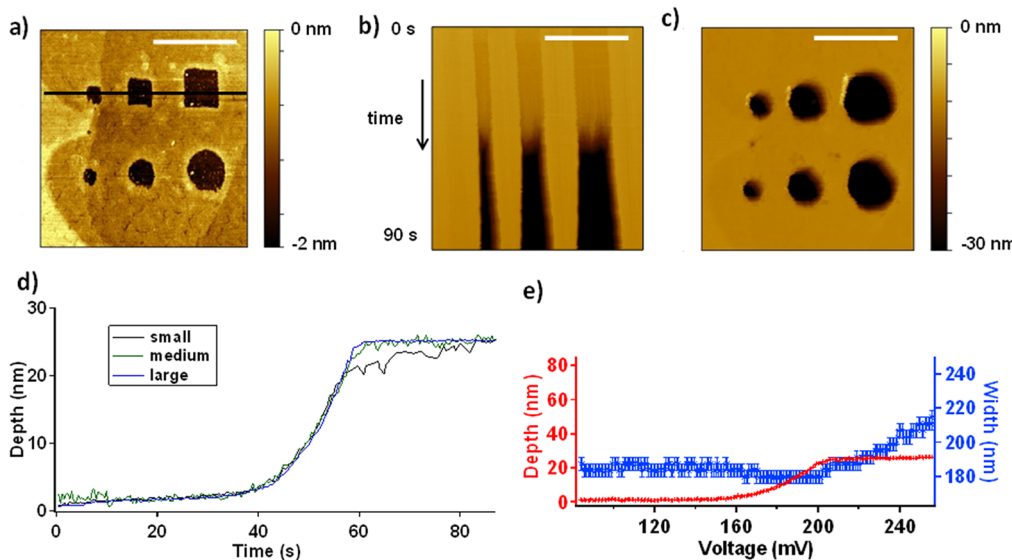


Figure 3. *In situ* measurement of patterns under linear potential sweep. (a) Different shapes were nanoshaved and the line indicated was imaged during etching. (b) AFM kymograph of the line in panel a, while a linear potential sweep was applied. The arrow shows the direction of the time axis. (c) AFM image of the nanoshaved shapes after etching, showing lateral expansion that is consistent with the kymograph in panel b. Panels b and c are shown on the same color scale. Some newly appeared bright features are observed in the first row, which are absent in other experiments where potential is kept below 210 mV. Therefore, these bright features may originate from products of decomposition reactions above 210 mV²⁷ or desorbed C18 molecules due to extensive lateral etching. As AFM tip may sweep these insoluble species along while collecting the kymograph, these species are more likely to accumulate near the imaged line. (d) The depth of three nanoshaved holes as a function of time. (e) Depth (red) and width (blue) of the largest hole as functions of potential. The onset of vertical etching occurred near 150 mV while lateral etching began near 200 mV. The uncertainty in potential measurement is approximately 10 mV. The uncertainty in width measurements is 4 nm as discussed in the Materials and Methods section. Scale bars are 400 nm in the AFM images.

Electrochemical Etching with a Linear Potential Sweep. To determine the onset potential of etching in the nanoshaved area, we applied a linear potential sweep from 85 ± 10 to 255 ± 10 mV at 2 mV/s to the nanoshaved surface under the thiourea solution (Figure 3a). The AFM kymograph of the squares (imaged line as marked in Figure 3a) was shown in Figure 3b. The image of the nanoshaved holes after etching (Figure 3c) shows that the holes were indeed expanded laterally, consistent with the kymograph. In addition, the extents of lateral expansion along different angles were similar. Hence the kymograph, which only measures the lateral expansion along one axis, is still a good representation of the lateral etching. The three squares had nearly identical depths over time, except that as the pattern etched deeper, there was some measured difference due to the tip convolution effect,³⁰ *i.e.*, the AFM tip could not reach the bottom of the smallest square (Figure 3d) during the scan. Therefore, the largest square was used to extract potential-dependent width and depth (Figure 3e). The lack of size dependence further supports that the etching is not mass transport limited. Due to the finite size of the tip, the crystallographic orientation of the sidewall could not be determined reliably. Future studies that use high aspect ratio AFM tips³¹ will be necessary to determine if the sidewall is vertical or slanted at a specific angle. The absolute width determination of the etched area can

be affected by the tip convolution.^{30,32} Nevertheless, the relative width change of the opening can be determined reliably, according to our estimate of the error caused by tip convolution (see Supporting Information). The onset of vertical etching (red symbols) occurred at 150 ± 10 mV, while lateral etching (blue symbols, error bars indicate the AFM measurement error) occurred at 200 ± 10 mV. The reason for such a lag will be discussed later. The inhibition of vertical etching at 200 ± 10 mV and above is consistent with existing studies showing that 210 mV triggers dimerization.²⁷ The dimerization leads to decomposition reactions and generates products that passivate the gold surface (Figure 3e).²⁷ On the other hand, the etching of the sidewall, which most likely has a different crystallographic plane, is unhindered at potentials above 200 mV.

Electrochemical Etching with a Potential Step. To understand etching at specific potentials in greater detail, we applied potential steps, 95 ± 10 , 109 ± 10 , and 172 ± 10 mV, respectively, to a surface with nanoshaved shapes that were identical to those in Figure 3a (shown in Figure 4a–c). The width and depth of the largest square were extracted and displayed in Figure 4d–f. The fact that in the potential step experiment, the etching begins below the onset potential determined in the potential sweep experiment can be attributed to the time required to reach a steady-state

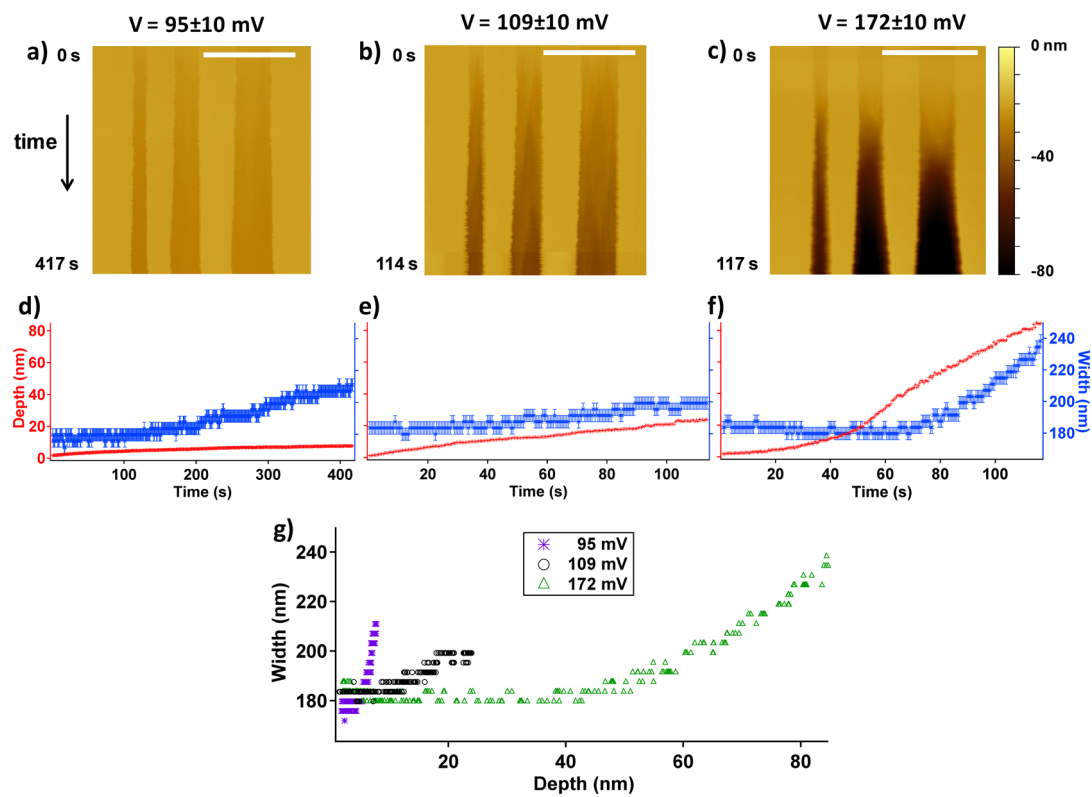
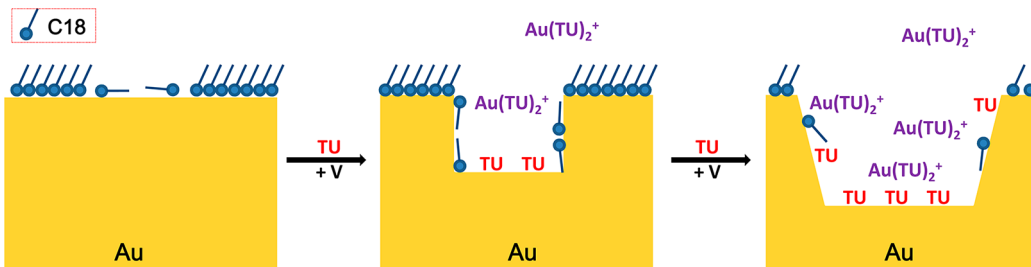


Figure 4. *In situ* measurement of patterns under different step potentials. (a–c) AFM kymographs of nanoshaved squares that were identical to Figure 3a and subjected to low (95 ± 10 mV), medium (109 ± 10 mV), and high (172 ± 10 mV) potential steps, respectively, being shown on the same color scale. As etch rate is relatively low at low and medium potentials, two consecutive AFM images are combined to analyze the kinetics. (d–f) Depth (red) and width (blue) evolution of the largest square over time for different step potentials, all shown with identical z scales. (g) Width vs depth plot at the three different step potentials. Scale bars are 400 nm.

etch rate after the potential is changed to a new value. Lateral etching was significant at all three potentials. However, a pronounced induction period for lateral etching was observed in these experiments. Hence, significant lateral etching occurred after the onset of vertical etching. The time lag is consistent with previous observations in the linear potential sweep experiment (Figure 3e). Interestingly, the etch depth beyond which lateral etching becomes significant, d_L , was dependent on the step potential (Figure 4g). At 95 and 109 mV, lateral etching began at a much smaller depth, 5 and 12 nm, respectively. By comparison, at 172 mV, lateral etching was undetectable (within the measurement error ~ 4 nm) until the depth of nanoshaved area exceeded 40 nm.

The large etching anisotropy implies that metal nanostructures with high aspect ratios can be produced with wet etching under optimized conditions. However, the anisotropy is unexpected considering that the more stable (111) facet (bottom of the hole) is typically etched more slowly.^{33–35} The origin of the preferential etching in the vertical direction remains to be fully understood. A plausible explanation is that residual adsorbates in the etched area have different interactions with the sidewall and the bottom

(Scheme 1). At a lower surface coverage, C18 molecules lie down to maximize the van der Waals contact between the alkyl chain and the gold surface,³⁶ impeding the complexation of thiourea with gold. Hence, the displacement of residual adsorbates may be the rate-limiting step in the etching reaction. Initially there is no lateral etching due to the absence of the side wall. However, once the first layer of gold in the nanoshaved area was etched, a sidewall with freshly exposed gold is generated. The etching of the sidewall allows lateral expansion of the nanoshaved area. While the bottom of the etched hole remains as (111) facet, the sidewall may have different crystallographic planes such as (110), which are known to bind thiol adsorbates more strongly than (111).^{35–37} By contrast, the adsorbates on the (111) facet are more readily displaced, kinetically favoring etching in the vertical direction. We found that prior to etching, the depth of the nanoshaved area was 0.6 nm smaller than expected given the thickness of C18 SAM (Figure 2e), which suggests the presence of adsorbates in the nanoshaved area. Numerous mechanisms could lead to the passivation of a freshly exposed sidewall. Given the high mobility of thiol molecules at low surface coverage,³⁶ the molecules diffuse from the nanoshaved areas to the sidewall,



Scheme 1. Proposed etching mechanism of nanoshaved pattern.

where the adsorption energy is higher. Additionally, if a minimal amount of lateral etching occurs, thiol molecules in the SAM at the edge of the nanoshaved area might detach and cap the sidewall of the etched hole. As the presence of low-coverage thiol molecules on exposed gold areas is common for SAM surfaces patterned with other techniques such as microcontact printing,¹⁰ dip-pen nanolithography¹³ and chemical lift-off lithography,¹⁵ due to the surface diffusion of thiols in additive methods,^{38,39} or incomplete removal of thiols in subtractive methods,¹⁵ the selective passivation of the sidewall, which can be exploited to promote anisotropic etching, may be a general phenomenon in wet etching with alkanethiol SAM resists.

That higher potentials allow the nanoshaved shapes to be etched to a greater d_L , the depth at the onset of lateral etching, may be explained by increased R_V , the vertical etch rate, at these potentials. d_L can be described by

$$d_L = \int_{t_V}^{t_L} R_V(t) dt$$

where t_V and t_L are the times when significant etching in vertical and lateral directions begins, respectively. At a higher potential where $R_V(t)$ is sharply increased,⁴⁰ significant vertical etching may occur between t_V and t_L . Although the time offset between vertical and lateral etching, $t_L - t_V$, may be potential dependent as well (about 140, 40, and 80 s for the low, medium, and high step potentials, respectively), $R_V(t)$ is much more sensitive to potential (increased by more than an order of magnitude when the potential increases from 95 to 172 mV).

In addition, we also evaluated the pattern transfer fidelity by looking for electrochemical etching through defects of SAM. This phenomenon was only observed when lateral etching is significant (Figures 2b and 3c) and mostly through large monolayer defects (Figures 2a and 3a). Figure S4 shows that even with significant lateral etching due to a prolonged period of time at 109 mV, etching in SAM defects is not observed. The minimal etching of gold in the SAM defects (Figure S4), which is consistent with a previous study,²⁵ may be attributed to the use of single crystalline substrate and thermal annealing protocol that additionally improves the order of the C18 SAM.

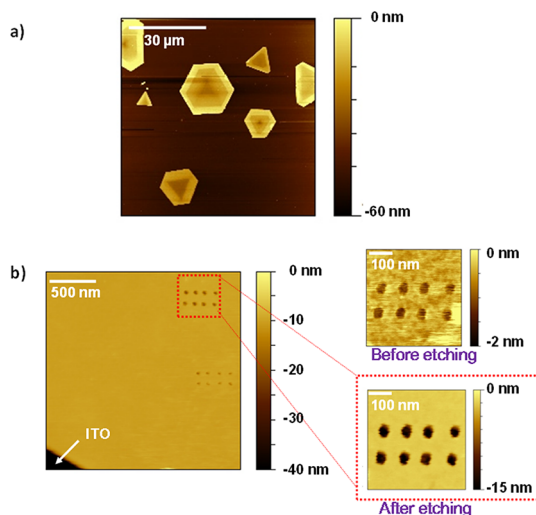


Figure 5. Application of electrochemical etching for fabrication of nanosized patterns. (a) AFM image of micrometer size single crystalline gold plates synthesized on top of ITO. The C18 SAM on the gold plates is patterned and etched. (b) AFM images showing circular nanoholes created by nanoshaving before and after etching. Note that etching through SAM defects was not observed. The two rows under highlighted areas are nanoshaved squares that have smaller area (about 30 nm wide) and were etched as well. However, the depth is smaller, which can be ascribed to the finite size of the tip, i.e., the tip could not reach the bottom of the small holes during imaging. AFM tips with higher aspect ratio would be needed to probe the depth of such small holes accurately.

The decrease in R_V at later stages of etching, as indicated by the slope change in depth vs time plots in Figures 3e and 4f, may originate from the accumulation of AuTU_2^+ in the etched hole. As the depth increases, the diffusion of AuTU_2^+ from the recessed etched hole to the bulk solution slows down, leading to the accumulation of the etching product that increases the backward reaction rate and reduces the net vertical etch rate.⁴⁰ Another possibility is the accumulation of side products that may passivate the bottom surface.²⁷ Numerical simulation of the diffusion and electrode reactions^{41,42} at the nanoscale will be needed to help clarify the origin.

Pattern Transfer on Gold Microplates. While studies on bulk single crystals offer important insight into the etching kinetics, the structures produced are of limited relevance to applications that exploit the plasmonic properties of gold, which often require thin films.^{43–45}

The gold microplates supported on indium–tin-oxide (ITO) are substrates that are single crystalline, inexpensive, compatible with electrochemistry, and have the required thicknesses (15–60 nm).²⁵ Because the top of the microplates is terminated with Au(111) and the plates can be readily functionalized with alkane-thiols,²⁵ we have explored the electrochemically controlled etching as a method to produce nanoholes in gold microplates. Figure 5 shows the AFM images of fabricated nanoholes near a corner of a gold plate after a step potential was applied to the substrate. Etching was carried out at 170 ± 10 mV to minimize lateral etching. The nanoholes generated this way were etched to 15 nm deep with lateral etching less than 5 nm. Due to the effective passivation of the SAM, the top surface remains atomically flat after etching, which should reduce the dampening of surface plasmons due to the roughness of polycrystalline thin films.⁴⁶

CONCLUSION

Our novel *in situ* method to probe the wet etching of gold at the nanoscale has yielded unique insight into the pattern transfer process on SAM resists. In *ex situ* electron microscopy and AFM studies, different samples must be withdrawn at different time points for microscopy characterization;^{10,12,13} the limited time resolution and sample-to-sample variability would preclude such detailed kinetics information obtained in this study. Notably we found that the etching rates of the bottom and sidewalls are not constant and have different onset times. Electrochemical potential can be

used to manipulate the etching kinetics and facilitate anisotropic etching with a ratio of at least 10:1. Although currently we do not know the ultimate etching anisotropy achievable because of the limited number of conditions explored, it is likely that even higher anisotropy can be obtained in a more systematic investigation.

Future studies that further elucidate the mechanistic details of the etching process, such as the roles of adsorbates, the crystallographic orientations of the sidewalls, other surfactant molecules to additionally suppress lateral etching, and the interplay between mass transport and electrode reactions at the nanoscale, may provide additional routes to suppress lateral etching and generate high-aspect ratio structures. With new insight of the nanoscale etching kinetics and inexpensive single crystalline Au microplate substrates,²⁵ wet etching with SAM resists could be a viable method to produce metal nanostructures with high precision. While our approach was demonstrated with nanoshaved SAM patterns, we expect it to be suitable for SAM patterns produced with other methods,⁴⁷ such as those combining high spatial resolution and high throughput.¹⁵ Since gold may only be exposed at sidewalls of the etched area while the rest of the substrate remains protected by a SAM, wet etching can potentially enable selective attachment of biochemical ligands to the etched holes or gaps (usually the EM “hot spots”), which remains challenging to achieve with existing techniques.^{8,9,44}

MATERIALS AND METHODS

Materials. Gold wire (99.99%, 1 mm diameter) was purchased from Scientific Instrument Services, Inc. 1-Octadecanethiol (C18, 98%) was purchased from Sigma-Aldrich. Ethanol (99.5%) and methyl sulfoxide (DMSO, 99.9%) were purchased from Acros Organics. Thiourea, sulfuric acid and other reagents were purchased from Fisher Scientific, Inc. and were of certified ACS or higher grade. Only ultrapure water ($>18\text{M}\Omega\cdot\text{cm}$) generated from a Barnstead Nanopure Diamond water purification system was used. All the glassware and parts used in the experiment were cleaned by piranha solution (1:3 $\text{H}_2\text{O}_2:\text{H}_2\text{SO}_4$) and rinsed copiously with water prior to use. (CAUTION: Piranha solution can react violently with organic materials, and should be handled with personal protective equipment. Piranha solution should not be stored in tightly sealed containers.)

Preparation of the Gold(111) Surface and Self-Assembled Monolayer. A single crystal gold bead with (111) facets was made by melting a gold wire and then mounted on a platinum foil.^{24,48} The gold bead was then cleaned by hot nitric acid and annealed by hydrogen flame, before immersion into a 2 mM C18 ethanol solution. To reduce the defects in the C18 monolayer, the container with sample in the thiol solution was purged with nitrogen, heated to 70 °C and gradually cooled down to room temperature overnight.⁴⁹ The gold sample was then briefly rinsed with ethanol and used immediately. The preparation of gold microplates on ITO and subsequent SAM growth were described in detail elsewhere.²⁵ Briefly, the gold plates were chemically synthesized on ITO by reducing Au(III) using ascorbic acid in the presence of capping agents, KI and

cetyltrimethylammonium bromide.²⁵ The capping agent iodide on gold plates was desorbed electrochemically at -800 mV and the C18 SAM on Au plates was prepared as mentioned above.

Electrochemical Etching. Potential control was applied either by an integrated potentiostat of the Agilent 5500 AFM or Epsilon from BASi (Bioanalytical Systems, Inc.). All the potential values quoted in this paper were measured *versus* Ag/AgCl (3 M KCl) electrode. The Pt quasi-reference electrode and Pt/Ir counter electrode were set up in the liquid cell at the beginning of the experiment. After nanoshaving, nitrogen purged 10 mM sulfuric acid was flushed through the liquid cell and a potential of -300 mV was applied. A solution containing 10 mM sulfuric acid and 40 mM thiourea was purged with nitrogen for 15 min and flushed through the liquid cell while the potential was kept at -300 mV to minimize etching. Electrode potential was applied when the pattern was repeatedly imaged by AFM. After the experiment, the quasi-reference electrode was calibrated using a commercial Ag/AgCl (3 M KCl) electrode from BASi. The voltage fluctuation in the calibration process was 10 mV and this value was used as the error in overall voltage measurement.

Atomic Force Microscopy. NT-MDT Solver Next AFM was used for general characterization of the gold microplates in air. An Agilent 5500 AFM, silicon probes (SNL-10, Bruker, 0.2–0.4 N/m) and a custom built Teflon liquid cell were used for nanoshaving and *in situ* imaging. The gold reflective coating on the AFM probes was removed by aqua regia before use to avoid etching of the coating in thiourea during *in situ* imaging. Nanoshaving was performed by using a protocol similar to that described in literature.¹⁸ Briefly, thiol molecules in selected regions of the C18 SAM were removed by applying high forces using the AFM

probe, in 1:1 (v/v) DMSO/water solution. The threshold of force required for AFM lithography was determined by progressively increasing the force until selective desorption was observed. Typical threshold forces applied, which depend on the sharpness of the AFM tip, range from 50 to 100 nN. To reduce the amount of residual C18 on the surface, double shaving in orthogonal directions were applied to the same pattern. The same tip was used for nanoshaving and imaging. Imaging of nanoshaved patterns in DMSO/water, butanol or ethanol was conducted in contact mode; otherwise, imaging was performed in tapping mode. An environmental chamber was used to maintain a nitrogen atmosphere during etching. The height measurements in AFM images were calibrated by atomic steps on Au(111) surface.

Data Analysis. AFM kymographs were imported into MATLAB and analyzed line-by-line to extract the width and depth of the etched area. Each imported image contains single shape. For each line, there are three steps to determine the width and depth: (1) the average height was calculated from data points in SAM region to determine the baseline height; (2) the deepest point in the hole was found as the depth of the pattern; (3) the boundary between etched area and SAM region was found by the Canny method⁵⁰ to calculate the width of the etched area.

There are several sources of error in the width measurement by AFM, tip convolution due to finite size of the AFM tip,^{30,32} pixel resolution (256 pixels for 1 μm length) and drift in y direction during AFM kymograph collection. The evaluation of the error due to tip convolution and pixel resolution can be found in the Supporting Information. To give a best estimate of the error due to y-direction drift, we analyzed the widths of the shaved area at different lines before etching, by making the assumption that each line would expand by the same extent during etching. The standard deviation of the pattern width is about 4 nm. Note that this value contains contribution from tip convolution and pixel resolution as well; therefore, we defined it as "AFM measurement error" and indicated it as the error bar for all the width measurement.

The time offset $t_i - t_f$ was estimated by extrapolation. The data points in width or depth measurement were divided into two regions, one without etching and one with significant etching. Then, a linear line was fit to each region and the intersection of the two fitted line was determined as the time offset.

Conflict of Interest: The authors declare no competing financial interest.

Acknowledgment. We acknowledge support from UC Merced and NSF (CHE 1048651). E.A.J. was supported by the UC Merced Faculty Mentor Program fellowship.

Supporting Information Available: Calculation of estimated etch rate, AFM measurement error, linear sweep voltammetry of bare gold in the etchant and additional AFM images. This material is available free of charge via the Internet at <http://pubs.acs.org>.

REFERENCES AND NOTES

- Jain, P. K.; Huang, X.; El-Sayed, I. H.; El-Sayed, M. A. Noble Metals on the Nanoscale: Optical and Photothermal Properties and Some Applications in Imaging, Sensing, Biology, and Medicine. *Acc. Chem. Res.* **2008**, *41*, 1578–1586.
- Grzelczak, M.; Pérez-Juste, J.; Mulvaney, P.; Liz-Marzán, L. M. Shape Control in Gold Nanoparticle Synthesis. *Chem. Soc. Rev.* **2008**, *37*, 1783–1791.
- Wiley, B.; Sun, Y.; Mayers, B.; Xia, Y. Shape-Controlled Synthesis of Metal Nanostructures: The Case of Silver. *Chem.—Eur. J.* **2005**, *11*, 454–463.
- Zhang, X.; Yonzon, C. R.; Van Duyne, R. P. Nanosphere Lithography Fabricated Plasmonic Materials and Their Applications. *J. Mater. Res.* **2006**, *21*, 1083–1092.
- Nagpal, P.; Lindquist, N. C.; Oh, S.; Norris, D. J. Ultrasmooth Patterned Metals for Plasmonics and Metamaterials. *Science* **2009**, *325*, 594–597.
- Huang, J.; Callegari, V.; Geisler, P.; Brüning, C.; Kern, J.; Prangsma, J. C.; Wu, X.; Feichtner, T.; Ziegler, J.; Weinmann, P. Atomically Flat Single-Crystalline Gold Nanostructures for Plasmonic Nanocircuitry. *Nat. Commun.* **2010**, *1*, 150.
- Liu, Z.; Steele, J. M.; Srituravanich, W.; Pikus, Y.; Sun, C.; Zhang, X. Focusing Surface Plasmons with a Plasmonic Lens. *Nano Lett.* **2005**, *5*, 1726–1729.
- Kinkhabwala, A.; Yu, Z.; Fan, S.; Avlasevich, Y.; Müllen, K.; Moerner, W. Large Single-Molecule Fluorescence Enhancements Produced by a Bowtie Nanoantenna. *Nat. Photonics* **2009**, *3*, 654–657.
- Beeram, S. R.; Zamborini, F. P. Selective Attachment of Antibodies to the Edges of Gold Nanostructures for Enhanced Localized Surface Plasmon Resonance Biosensing. *J. Am. Chem. Soc.* **2009**, *131*, 11689–11691.
- Xia, Y.; Zhao, X. M.; Kim, E.; Whitesides, G. M. A Selective Etching Solution for use with Patterned Self-Assembled Monolayers of Alkanethiolates on Gold. *Chem. Mater.* **1995**, *7*, 2332–2337.
- Salaita, K. S.; Lee, S. W.; Ginger, D. S.; Mirkin, C. A. DPN-Generated Nanostructures as Positive Resists for Preparing Lithographic Masters or Hole Arrays. *Nano Lett.* **2006**, *6*, 2493–2498.
- Wei, J. H.; Ginger, D. S. A Direct-Write Single-Step Positive Etch Resist for Dip-Pen Nanolithography. *Small* **2007**, *3*, 2034–2037.
- Lu, G.; Chen, Y.; Li, B.; Zhou, X.; Xue, C.; Ma, J.; Boey, F. Y. C.; Zhang, H. Dip-Pen Nanolithography-Generated Patterns used as Gold Etch Resists: A Comparison Study of 16-Mercaptohexadecanoic Acid and 1-Octadecanethiol. *J. Phys. Chem. C* **2009**, *113*, 4184–4187.
- Wilbur, J. L.; Kumar, A.; Kim, E.; Whitesides, G. M. Micro-fabrication by Microcontact Printing of Self-Assembled Monolayers. *Adv. Mater.* **1994**, *6*, 600–604.
- Liao, W.; Cheunkar, S.; Cao, H. H.; Bednar, H. R.; Weiss, P. S.; Andrews, A. M. Subtractive Patterning via Chemical Lift-Off Lithography. *Science* **2012**, *337*, 1517–1521.
- Nyffenegger, R. M.; Penner, R. M. Nanometer-Scale Surface Modification Using the Scanning Probe Microscope: Progress since 1991. *Chem. Rev.* **1997**, *97*, 1195–1230.
- Piner, R. D.; Zhu, J.; Xu, F.; Hong, S. H.; Mirkin, C. A. "Dip-Pen" Nanolithography. *Science* **1999**, *283*, 661–663.
- Liu, G. Y.; Xu, S.; Qian, Y. L. Nanofabrication of Self-Assembled Monolayers Using Scanning Probe Lithography. *Acc. Chem. Res.* **2000**, *33*, 457–466.
- Yu, Q.; Guan, P.; Qin, D.; Golden, G.; Wallace, P. M. Inverted Size-Dependence of Surface-Enhanced Raman Scattering on Gold Nanohole and Nanodisk Arrays. *Nano Lett.* **2008**, *8*, 1923–1928.
- Jain, P. K.; Huang, W.; El-Sayed, M. A. On the Universal Scaling Behavior of the Distance Decay of Plasmon Coupling in Metal Nanoparticle Pairs: A Plasmon Ruler Equation. *Nano Lett.* **2007**, *7*, 2080–2088.
- Geissler, M.; Wolf, H.; Stutz, R.; Delamarche, E.; Grummt, U.; Michel, B.; Bietsch, A. Fabrication of Metal Nanowires using Microcontact Printing. *Langmuir* **2003**, *19*, 6301–6311.
- Zamborini, F. P.; Crooks, R. M. *In Situ* Electrochemical Scanning Tunneling Microscopy (ECSTM) Study of Cyanide-Induced Corrosion of Naked and Hexadecyl Mercaptan-Passivated Au(111). *Langmuir* **1997**, *13*, 122–126.
- Zamborini, F. P.; Crooks, R. M. Corrosion Passivation of Gold by N-Alkanethiol Self-Assembled Monolayers: Effect of Chain Length and End Group. *Langmuir* **1998**, *14*, 3279–3286.
- Clavilier, J.; Faure, R.; Guinet, G.; Durand, R. Preparation of Monocrystalline Pt Microelectrodes and Electrochemical Study of the Plane Surfaces Cut in the Direction of the {111} and {110} Planes. *J. Electroanal. Chem. Interfacial Electrochem.* **1979**, *107*, 205–209.
- Lee, C.; Josephs, E. A.; Shao, J.; Ye, T. Nanoscale Chemical Patterns on Gold Microplates. *J. Phys. Chem. C* **2012**, *116*, 17625–17632.
- Zhang, H.; Mirkin, C. A. DPN-Generated Nanostructures made of Gold, Silver, and Palladium. *Chem. Mater.* **2004**, *16*, 1480–1484.
- Lin, J. C.; Huarng, J. J. Electrochemical Stripping of Gold from Au-Ni-Cu Electronic Connector Scrap in an Aqueous

Solution of Thiourea. *J. Appl. Electrochem.* **1994**, *24*, 157–165.

28. Kazakov, V.; Lapshin, A.; Peshchevitskii, B. Redox Potential of the Gold(II) Thiourea Complex. *Russ. J. Inorg. Chem.* **1964**, *9*, 708–709.

29. Groenewald, T. The Dissolution of Gold in Acidic Solutions of Thiourea. *Hydrometallurgy* **1976**, *1*, 277–290.

30. Tranchida, D.; Piccarolo, S.; Deblieck, R. Some Experimental Issues of AFM Tip Blind Estimation: The Effect of Noise and Resolution. *Meas. Sci. Technol.* **2006**, *17*, 2630.

31. Wilson, N. R.; Macpherson, J. V. Carbon Nanotube Tips for Atomic Force Microscopy. *Nat. Nanotechnol.* **2009**, *4*, 483–491.

32. Wilson, D. L.; Kump, K. S.; Eppell, S. J.; Marchant, R. E. Morphological Restoration of Atomic Force Microscopy Images. *Langmuir* **1995**, *11*, 265–272.

33. Mulvihill, M. J.; Ling, X. Y.; Henzie, J.; Yang, P. Anisotropic Etching of Silver Nanoparticles for Plasmonic Structures Capable of Single-Particle SERS. *J. Am. Chem. Soc.* **2009**, *132*, 268–274.

34. Wang, Z. Transmission Electron Microscopy of Shape-Controlled Nanocrystals and their Assemblies. *J. Phys. Chem. B* **2000**, *104*, 1153–1175.

35. Desai, K. R. *Surface Chemistry*; Oxford Book Co.: New York, 2008; pp 1–25.

36. Vericat, C.; Vela, M.; Benitez, G.; Carro, P.; Salvarezza, R. Self-Assembled Monolayers of Thiols and Dithiols on Gold: New Challenges for a Well-Known System. *Chem. Soc. Rev.* **2010**, *39*, 1805–1834.

37. Rzeznicka, I. I.; Lee, J.; Maksymovich, P.; Yates, J. T., Jr. Non-dissociative Chemisorption of Short Chain Alkanethiols on Au(111). *J. Phys. Chem. B* **2005**, *109*, 15992–15996.

38. Delamarche, E.; Schmid, H.; Bietsch, A.; Larsen, N.; Rothuizen, H.; Michel, B.; Biebuyck, H. Transport Mechanisms of Alkanethiols during Microcontact Printing on Gold. *J. Phys. Chem. B* **1998**, *102*, 3324–3334.

39. Sheehan, P.; Whitman, L. Thiol Diffusion and the Role of Humidity in “Dip Pen Nanolithography. *Phys. Rev. Lett.* **2002**, *88*, 156104.

40. Bard, A. J.; Faulkner, L. R. *Electrochemical Methods: Fundamentals and Applications*; Wiley: New York: 1980; pp 87–136.

41. Bartlett, P.; Taylor, S. An Accurate Microdisc Simulation Model for Recessed Microdisc Electrodes. *J. Electroanal. Chem.* **1998**, *453*, 49–60.

42. Guo, J.; Lindner, E. Cyclic Voltammetry at Shallow Recessed Microdisc Electrode: Theoretical and Experimental Study. *J. Electroanal. Chem.* **2009**, *629*, 180–184.

43. Lakowicz, J. R. Radiative Decay Engineering: Biophysical and Biomedical Applications. *Anal. Biochem.* **2001**, *298*, 1.

44. Brolo, A. G.; Arctander, E.; Gordon, R.; Leathem, B.; Kavanagh, K. L. Nanohole-Enhanced Raman Scattering. *Nano Lett.* **2004**, *4*, 2015–2018.

45. Vaish, A.; Liao, W.; Shuster, M. J.; Hinds, J. M.; Weiss, P. S.; Andrews, A. M. Thin Gold Film-Assisted Fluorescence Spectroscopy for Biomolecule Sensing. *Anal. Chem.* **2011**, *83*, 7451–7456.

46. Chen, K.; Drachev, V. P.; Borneman, J. D.; Kildishev, A. V.; Shalaev, V. M. Drude Relaxation Rate in Grained Gold Nanoantennas. *Nano Lett.* **2010**, *10*, 916–922.

47. Smith, R. K.; Lewis, P. A.; Weiss, P. S. Patterning Self-Assembled Monolayers. *Prog. Surf. Sci.* **2004**, *75*, 1–68.

48. Josephs, E. A.; Ye, T. A Single-Molecule View of Conformational Switching of DNA Tethered to a Gold Electrode. *J. Am. Chem. Soc.* **2012**, *134*, 10021–10030.

49. Bucher, J. P.; Santesson, L.; Kern, K. Thermal Healing of Self-Assembled Organic Monolayers: Hexane- and Octadecanethiol on Au(111) and Ag(111). *Langmuir* **1994**, *10*, 979–983.

50. Canny, J. A Computational Approach to Edge Detection. *IEEE Trans. Pattern Anal. Mach. Intell.* **1986**, *6*, 679–698.